Artificial Life and Robotics (2018) 23:515–522
https://doi.org/10.1007/s10015-018-0479-1

ORIGINAL ARTICLE

Helical wave propagation motion for a snake robot on a vertical pipe containing a branch

Wei Qi[1] · Tetsushi Kamegawa[2] · Akio Gofuku[2]

Received: 8 February 2018 / Accepted: 26 July 2018 / Published online: 26 September 2018

Abstract
Snake robots could be utilized in many fields because of their hyper-redundant properties, although there are still control problems when they are operated in complex environments. For example, a helical rolling motion has been used to climb a pipe. By using this kind of motion, a snake robot can move along the inside or outside of a pipe. However, this motion has limitations when the robot moves along a pipe containing a high gap or a branch point. In this study, we propose a type of motion for snake robots that involves wrapping around the outside of a pipe to overcome a branch point on it. This new motion uses a hyperbolic function to make a helical wave curve, which is then propagated by shifting the shape of the hyperbolic function along the body of the snake robot. The joint angles of the snake robot are derived by calculating the curvature and torsion of the curve on the basis of the formula of the continuous curve model. Finally, the results of simulations performed using the Robot Operating System and Gazebo programs are shown to validate the effectiveness of the new motion.

Keywords Helical wave propagation motion · Snake robot · Hyperbolic function

1 Introduction

Although the form of a biological snake is simple, snakes can move in various environments using several methods. They can also grip an object by wrapping around it and moving along it. It is considered that the development of a robot that mimics the characteristics of biological snakes, which can perform various tasks in simple forms, could have significant advantages. Until now, several kinds of mechanisms and controllers for snake robots have been studied. Hirose et al. revealed the principle of the undulatory curve of a biological snake and called it a serpenoid curve. Moreover, on the basis of the finding that biological snakes are propelled by frictional differences between the tangential and normal directions on their trunk, a smooth, undulatory snake robot motion with passive wheels has been realized [1, 2]. Thereafter, to extend the configuration space of snake robots to 3D space, devices constructed by alternately combining pitch and yaw axes were developed. With these robots, various motion, such as sidewinding, lateral rolling, and helical rolling motions, have been realized [3–5]. Sidewinding motion is observed as the locomotion of snakes in the desert when they move across loose or slippery environments. Lateral rolling and helical rolling motions are rarely seen in biological snakes; thus, these motions are considered as unique snake robot motions. In particular, the motion called helical rolling motion is utilized to move along the inside or outside a pipe [6–8]. This type of motion allows movement along a pipe by twisting the snake robot's trunk in a state of coiling around that pipe. However, this motion is unsuitable if there is a branch on the pipe; if that is the case, the snake robot is no longer able to move forward across the branch. In this research, we aim to develop a snake robot movement that involves wrapping around the outside of a pipe to overcome a branch point on that pipe. To move across the branch, we propose a new

This work was presented in part at the 2nd International Symposium on Swarm Behavior and Bio-Inspired Robotics, Kyoto, October 29–November 1, 2017.

✉ Wei Qi
qi.w.mif@s.okayama-u.ac.jp

[1] Graduate School of Natural Science and Technology, Okayama University, 3-1-1 Tsushimanaka, Kita-ku, Okayama, Japan

[2] Graduate School of Interdisciplinary Science and Engineering in Health Systems, Okayama University, 3-1-1 Tsushimanaka, Kita-ku, Okayama, Japan

motion that we call helical wave propagation motion. This type of motion is also a unique motion of snake robots. The helical wave curve is propagated by shifting the shape of the hyperbolic function; as far as we know, this is a new method for propagating a snake robot to the tangential direction along its body. In this paper, the design of the helical wave curve is formulated, and the curve is incorporated into the Frenet–Serret continuous curve model. Furthermore, the initial twisting value at the robot's end is appropriately calculated to achieve a consistent shift motion. The effectiveness of the motion is verified by simulations.

2 Helical rolling motion based on the continuous curve model

When planning a snake robot's motion, a method that uses the curvature and torsion of the snake's trunk (expressed as a continuous curve model) is often used. The derivation of target joint angles for snake robots from a continuous curve model has been presented in the previous publications [9, 10]. The target angles of the snake robot's joints are applied to a mechanical system to realize the planned motion. The outline of the method for a helical rolling motion is described below. The helical shape is a basic shape for achieving helical wave propagation motion and will be described in detail in later parts of the paper.

2.1 Mathematical continuum model

A continuum curve in 3D space is expressed by the Frenet–Serret equation, which expresses a curve $\mathbf{c}(s)$ using curvature $\kappa(s)$ and torsion $\tau(s)$.

$$\begin{cases} \mathrm{d}\mathbf{c}(s)/\mathrm{d}s &= \mathbf{e_1}(s) \\ \mathrm{d}\mathbf{e_1}(s)/\mathrm{d}s &= \kappa(s)\mathbf{e_2}(s) \\ \mathrm{d}\mathbf{e_2}(s)/\mathrm{d}s &= -\kappa(s)\mathbf{e_1}(s) + \tau(s)\mathbf{e_3}(s) \\ \mathrm{d}\mathbf{e_3}(s)/\mathrm{d}s &= -\tau(s)\mathbf{e_2}(s) \end{cases} \tag{1}$$

where s is a parameter of length along the curve. $\mathbf{e_1}(s)$, $\mathbf{e_2}(s)$, and $\mathbf{e_3}(s)$ are orthonormal basis unit vectors. $\mathbf{e_1}(s)$ is a tangential vector to the curve at s, $\mathbf{e_2}(s)$ is a vector that indicates the direction of changing the curve at s, and $\mathbf{e_3}(s)$ is a vector that is given by $\mathbf{e_3}(s) = \mathbf{e_1}(s) \times \mathbf{e_2}(s)$ as shown in Fig. 1.

However, the Frenet–Serret formulation is not suitable for a snake robot's coordinate system because Frenet–Serret only gives the shape of the curved line, whereas a snake robot's coordinate system should correspond to the joint structure of the robot. By taking into account that a mechanical snake robot's coordinate system $\mathbf{e_r}(s)$, $\mathbf{e_p}(s)$, $\mathbf{e_y}(s)$ is introduced in Fig. 2, let $\tau_{\mathrm{roll}}(s)$, $\kappa_{\mathrm{pitch}}(s)$, and $\kappa_{\mathrm{yaw}}(s)$ be the torsion of roll, curvature of pitch, and curvature of yaw at point s on the continuum robot's coordinate system, respectively.

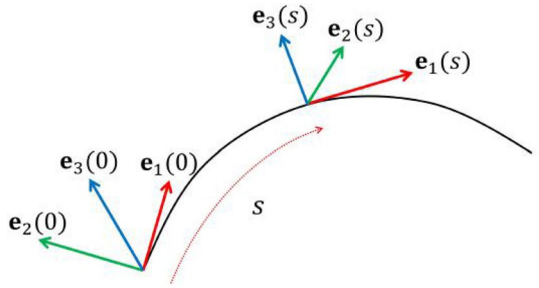

Fig. 1 Coordinate system for Frenet–Serret

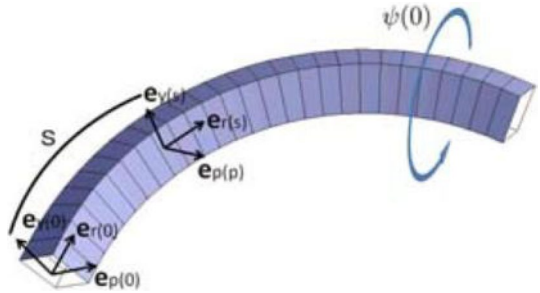

Fig. 2 Illustration of the coordinate system for a snake robot

In this formulation, the continuum curve is given by the following equations:

$$\begin{cases} \mathrm{d}\mathbf{c}(s)/\mathrm{d}s = \mathbf{e_r}(s) \\ \mathrm{d}\mathbf{e_r}(s)/\mathrm{d}s = \kappa_{\mathrm{yaw}}(s)\mathbf{e_p}(s) - \kappa_{\mathrm{pitch}}(s)\mathbf{e_y}(s) \\ \mathrm{d}\mathbf{e_p}(s)/\mathrm{d}s = -\kappa_{\mathrm{yaw}}(s)\mathbf{e_r}(s) + \tau_{\mathrm{roll}}(s)\mathbf{e_y}(s) \\ \mathrm{d}\mathbf{e_y}(s)/\mathrm{d}s = \kappa_{\mathrm{pitch}}(s)\mathbf{e_r}(s) - \tau_{\mathrm{roll}}(s)\mathbf{e_p}(s) \end{cases} \tag{2}$$

In this formula, $\tau_{\mathrm{roll}}(s)$, $\kappa_{\mathrm{pitch}}(s)$, and $\kappa_{\mathrm{yaw}}(s)$ determine the shape of the continuum curve in 3D space.

The snake robot in this paper has only pitch and yaw axes. These is no roll axis, therefore, $\tau_{\mathrm{roll}}(s)$ in Eq. (2) is $\tau_{\mathrm{roll}}(s) = 0$. Equation (2) then becomes the following:

$$\begin{cases} \mathrm{d}\mathbf{c}(s)/\mathrm{d}s &= \mathbf{e_r}(s) \\ \mathrm{d}\mathbf{e_r}(s)/\mathrm{d}s &= \kappa_{\mathrm{yaw}}(s)\mathbf{e_p}(s) - \kappa_{\mathrm{pitch}}(s)\mathbf{e_y}(s) \\ \mathrm{d}\mathbf{e_p}(s)/\mathrm{d}s &= -\kappa_{\mathrm{yaw}}(s)\mathbf{e_r}(s) \\ \mathrm{d}\mathbf{e_y}(s)/\mathrm{d}s &= \kappa_{\mathrm{pitch}}(s)\mathbf{e_r}(s) \end{cases} \tag{3}$$

Let $\psi(s)$ be the angle difference between $\mathbf{e_2}(s)$ and $\mathbf{e_p}(s)$ Fig. 3. According to Fig. 3, the following equations are obtained as a rotation around vector:

$$\begin{cases} \mathbf{e_p}(s) = \mathbf{e_2}(s)\cos\psi(s) - \mathbf{e_3}(s)\sin\psi(s) \\ \mathbf{e_y}(s) = \mathbf{e_2}(s)\sin\psi(s) + \mathbf{e_3}(s)\cos\psi(s) \end{cases} \tag{4}$$

Equation (5) is derived as $\mathbf{e_1}(s) = \mathbf{e_r}(s)$ from Eqs. (1) and (3).

$$\kappa(s)\mathbf{e_2}(s) = \kappa_{\mathrm{yaw}}(s)\mathbf{e_p}(s) - \kappa_{\mathrm{pitch}}(s)\mathbf{e_y}(s) \tag{5}$$

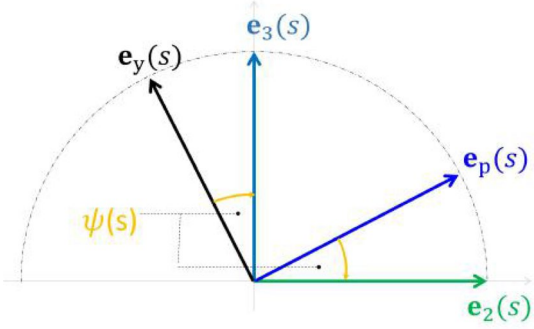

Fig. 3 $\psi(s)$: difference of angle between $\mathbf{e_2}(s)$ and $\mathbf{e_p}(s)$

and the following equations are obtained by substituting Eq. (4) in Eq. (5) and considering the coefficients $\mathbf{e_2}(s)$ and $\mathbf{e_3}(s)$:

$$\begin{cases} \kappa(s) = \kappa_{\text{yaw}}(s)\cos\psi(s) - \kappa_{\text{pitch}}(s)\sin\psi(s) \\ 0 = \kappa_{\text{yaw}}(s)\sin\psi(s) + \kappa_{\text{pitch}}(s)\cos\psi(s) \end{cases} \tag{6}$$

Furthermore, Eq. (7) is derived from Eqs. (1), (3), and (4) :

$$\begin{aligned} \frac{\mathrm{d}(\mathbf{e_2}(s)\mathbf{e_p}(s))}{\mathrm{d}s} &= \frac{\mathrm{d}\mathbf{e_2}(s)}{\mathrm{d}s}\mathbf{e_p}(s) + \mathbf{e_2}(s)\frac{v\mathbf{e_p}(s)}{\mathrm{d}s} \\ &= -\tau\sin\psi(s) \end{aligned} \tag{7}$$

From $\mathbf{e_2}(s)\cdot\mathbf{e_p}(s) = \cos\psi(s)$ and Eq. (7), we obtain Eq. (8):

$$\begin{aligned} \frac{\mathrm{d}\cos\psi(s)}{\mathrm{d}s} &= \frac{\mathrm{d}\psi(s)}{\mathrm{d}s}\sin\psi(s) \\ &= -\tau\sin\psi(s)\frac{\mathrm{d}\psi(s)}{\mathrm{d}s} = \tau(s) \end{aligned} \tag{8}$$

Therefore, the expressions of $\kappa_{\text{yaw}}(s)$ and $\kappa_{\text{pitch}}(s)$ using $\kappa(s)$ and $\tau(s)$ are derived by Eqs. (6) and (8) as follows :

$$\begin{cases} \kappa_{\text{pitch}}(s) &= -\kappa(s)\sin(\psi(s)) \\ \kappa_{\text{yaw}}(s) &= \kappa(s)\cos(\psi(s)) \\ \psi(s) &= \displaystyle\int_0^s \tau(s)\mathrm{d}s + \psi(0) \end{cases} \tag{9}$$

where $\psi(0)$ is an integral constant value at time t, which can be arbitrarily decided by an operator to obtain a rolling motion.

2.2 Design of helical shape and rolling motion

The helical shape is expressed as follows in Cartesian coordinates:

$$\begin{cases} x(t) = a\cos(t) \\ y(t) = a\sin(t) \\ z(t) = b(t) \end{cases} \tag{10}$$

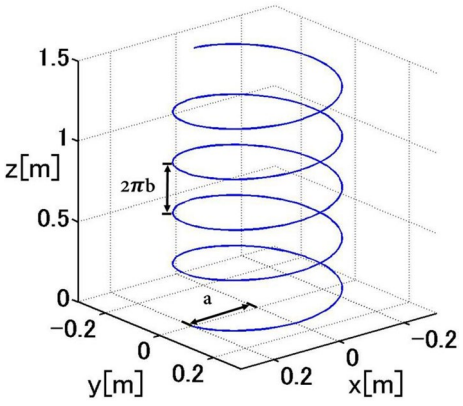

Fig. 4 An example of a helical shape ($a = 0.2$, $b = 0.05$)

where a denotes the helical radius, b is the increasing ratio of helical shape in the z direction, and t is a parameter. An example of a helical shape that is generated from Eq. (10) is shown in Fig. 4. After the design of the helical shape in the Cartesian coordinate system, the target shape is converted to a curve in the Frenet–Serret equation. The curvature and torsion of the curve are obtained from the geometrical conditions given by the following equations:

$$\kappa(t) = \frac{\sqrt{(\dot{y}\ddot{z} - \dot{z}\ddot{y})^2 + (\dot{z}\ddot{x} - \dot{x}\ddot{z})^2 + (\dot{x}\ddot{y} - \dot{y}\ddot{x})^2}}{(\dot{x}^2 + \dot{y}^2 + \dot{z}^2)^{\frac{3}{2}}} \tag{11}$$

$$\tau(t) = \frac{x^{(3)}(\dot{y}\ddot{z} - \dot{z}\ddot{y}) + y^{(3)}(\dot{z}\ddot{x} + \dot{x}\ddot{z}) + z^{(3)}(\dot{x}\ddot{y} + \dot{y}\ddot{x})}{(\dot{y}\ddot{z} - \dot{z}\ddot{y})^2 + (\dot{z}\ddot{x} - \dot{x}\ddot{z})^2 + (\dot{x}\ddot{y} - \dot{y}\ddot{x})^2} \tag{12}$$

where $\dot{x}$, $\ddot{x}$ and $x^{(3)}$ denote the first-, second-, and third-order differentiation with respect to t, respectively. By substituting Eq. (10) in Eqs. (11) and (12), we obtain the curvature and torsion:

$$\kappa(t) = \frac{a}{a^2 + b^2} \tag{13}$$

$$\tau(t) = \frac{b}{a^2 + b^2} \tag{14}$$

From Eqs. (13) and (14), it is found that the curvature and torsion of the helical shape have constant values with respect to parameter t. They also have the same constant values with respect to parameter s. By changing the values of a and b in Eq. (10), the radius and pitch of the helical shape can be designed. Furthermore, by changing the value of $\psi(0)$, the continuum robot's coordinate system is rolled around $\mathbf{e_r}(s)$ such that the robot generates a lateral rolling motion.

2.3 Application to a discrete mechanical snake robot model

According to the definition of curvature, the degrees of relative rotation for the pitch and yaw joints of the robot's coordinate system are expressed by $\kappa_{\text{pitch}}(s)\mathrm{d}s$ and $\kappa_{\text{yaw}}(s)\mathrm{d}s$, respectively. Therefore, if the length between the pitch and yaw joints of a discrete mechanical snake robot is δs, the desired angle of the i-th joint θ_i^d is expressed as follows :

$$\theta_i^d = \begin{cases} 2\delta s \cdot \kappa_{\text{yaw}}(i\delta s)(i : \text{odd joint}) \\ 2\delta s \cdot \kappa_{\text{pitch}}(i\delta s)(i : \text{even joint}) \end{cases} \tag{15}$$

In this study, odd-number joints are yaw joints, and even-number joints are pitch joints. The coefficient "2" indicates that the interval of pitch and yaw joints is $2\delta s$.

2.4 Problems of the helical rolling motion

Snake robots can move along cylindrical objects using the helical rolling motion, which is a type of motion that allows travel along a pipe by twisting the snake robot's trunk in the state of coiling around that pipe. Although there are a few research reports about movement on a pipe by means of helical rolling motion, there are still several problems related to this type of motion.

In particular, a snake robot cannot overcome a part of a pipe that contains a branch point, as shown in Fig. 5. The snake robot never crosses a branch point as long as it moves in a binormal direction to its body. To address this issue, we consider making the snake robot move in a tangential direction along its body, as shown in Fig. 6, rather than in a binormal direction by helical rolling motion.

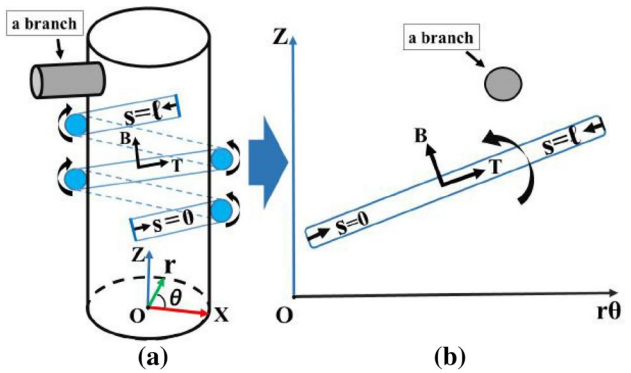

Fig. 5 Illustration of helical rolling motion: $s = l$ is the head of the snake robot, and $s = 0$ is the tail of the snake robot; B is the binormal direction, and T is the tangential direction along the snake robot's body. (a) The state of a snake robot climbing a pipe through helical rolling motion. (b) The state is projected in the z-$r\theta$ plane. In this plane, the shape of the snake robot is a line

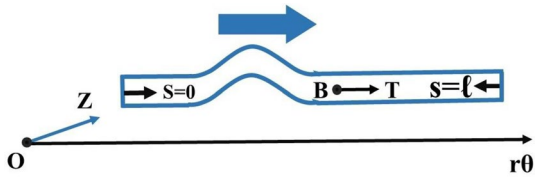

Fig. 6 Helical wave propagation motion

3 Formulation of helical wave curves

3.1 Design of a helical wave curve

At first, it is assumed that a snake robot is in a state of wrapping around a pipe. Thereafter, it creates a longitudinal wave to float parts of its trunk from the pipe. The float parts are transmitted from the tail to the head of a snake robot by a shifting method described later. In this study, the helical wave curve is expressed in Cartesian coordinates as follows:

$$\begin{cases} x(t) = a(t)\cos(t) \\ y(t) = a(t)\sin(t) \\ z(t) = b(t) \end{cases} \tag{16}$$

$$\begin{aligned} a(t) &= \rho(t) + r \\ b(t) &= \frac{n}{2\pi}t \end{aligned} \tag{17}$$

$$\begin{aligned} &\rho(t) = A\,\mathrm{sech}(\omega t - \phi) \\ &\{A \in \mathcal{R} \mid A > 0\}, \{\omega \in \mathcal{R} \mid \omega > 0\}, \phi \in \mathcal{R} \end{aligned} \tag{18}$$

where r is the radius of a helical curve, n is a pitch in the z-axis direction of the helical curve, and t is a parameter. It is very important to identify the appropriate $a(t)$ to modify an ordinary helical curve. To make the longitudinal wave that floats parts of the trunk from a pipe, we design $a(t)$ as a hyperbolic function of sech added to the radius r.

In the hyperbolic function, A is the amplitude, ω is the period, and ϕ is the initial phase, as shown in Fig. 7. If parameter A is increased, the ordinates of the curve increase A times. If parameter ω is increased, the abscissas of the curve decrease $1/\omega$ times. Furthermore, the curve can be moved to the left or the right by changing the value of ϕ.

3.2 Derivation of curvature κ and torsion τ

After the design of the helical wave curve in the Cartesian coordinate system, the target shape is converted to a curve in the Frenet–Serret equation Eq. (1). The curvature and torsion of the curve are obtained from the geometrical conditions in Eqs. (11) and (12).

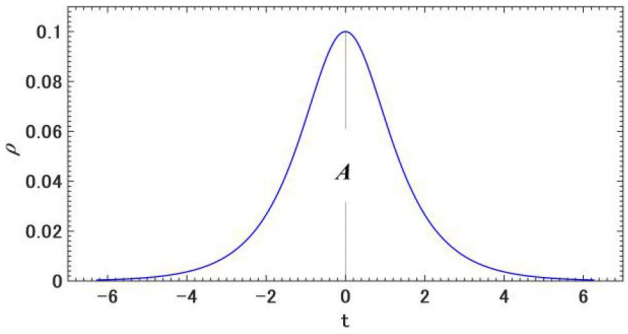

Fig. 7 Examples of hyperbolic function of sech ($A = 0.1$C$\omega = 1$ C$\phi = 0\pi$, domain $[-2\pi, 2\pi]$)

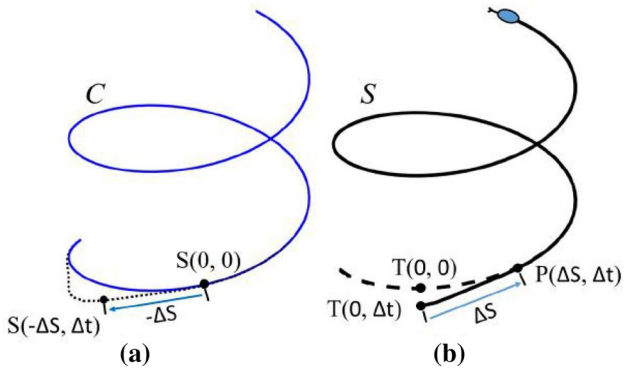

Fig. 8 Helical wave curve and snake robot shape: **a** planned curve; **b** application to a snake robot at Δt

Note that the curvature and torsion of the curve obtained using Eqs. (11) and (12) are a function of parameter t. To calculate the target angle of each joint of the snake robot using Eq. (1) of the Frenet–Serret formula, $\kappa(s)$ and $\tau(s)$ should be a function of the length parameter s of the curve.

Therefore, the curvature $\kappa(t)$ and torsion $\tau(t)$ should be converted to $\kappa(s)$ and $\tau(s)$ by taking into account the relationship between the length parameter s and parameter t. By setting the starting point of the curve at $t = 0$, the length s between $t = 0$ and $t = \theta$ of the curve is given by the formula of the path integral of the following equation :

$$s(\theta) = \int_0^{\theta} \sqrt{\left(\frac{\mathrm{d}x(t)}{\mathrm{d}t}\right)^2 + \left(\frac{\mathrm{d}y(t)}{\mathrm{d}t}\right)^2 + \left(\frac{\mathrm{d}z(t)}{\mathrm{d}t}\right)^2}\,\mathrm{d}t \tag{19}$$

The part in the root is simplified by substituting Eq. (16) into Eq. (19):

$$\begin{aligned}&\left(\frac{\mathrm{d}x(t)}{\mathrm{d}t}\right)^2 + \left(\frac{\mathrm{d}y(t)}{\mathrm{d}t}\right)^2 + \left(\frac{\mathrm{d}z(t)}{\mathrm{d}t}\right)^2 \\ &= \left(\frac{\mathrm{d}a(t)}{\mathrm{d}t}\right)^2 + (a(t))^2 + \left(\frac{\mathrm{d}b(t)}{\mathrm{d}t}\right)^2\end{aligned} \tag{20}$$

3.3 Wave propagation

At first, a hyperbolic function is designed to achieve an appropriate size of the wave by changing the parameters in Eq. (18). The width of the wave is almost $4\pi/\omega$, according to Fig. 7. To gradually add the floated longitudinal wave to the helical curve, the initial point of the wave should be $\phi = 2\pi/\omega$. Thereafter, the parameters to make the wave is shifted from the tail to the head of the snake robot along its body by a shift-control method. In this shift-control method, the parameters for the tail part should be given in the next step. A helical wave curve and a snake robot's shape at the initial state are shown in Fig. 8. In Fig. 8a, the pre-planned helical shape is represented by a solid line, whereas the dotted line shows the additional helical wave curve. In this figure, the tail part is located at $S(0, 0)$. In the next step, after Δt, the parameter for the tail part is given by $S(-\Delta s, \Delta t)$. Δs is a small section to the next part on the planned curve and is defined such that the direction to the head is "plus". Fig. 8b shows the shape of a snake robot at time Δt, and the broken line is the shape of the original helical curve. Let $\kappa_c(0, 0)$ and $\psi_c(0, 0)$ be parameters of curvature and twisting amount at $s = 0$ and $t = 0$ on the planned curve C.

Furthermore, let $\kappa_s(0, 0)$ and $\psi_s(0, 0)$ be parameters of the curvature and twisting amount at the tail part $T(0, 0)$ of the snake robot. Note that at the tail position, s is always zero. At time $t = \Delta t$, parameters $\kappa_c(-\Delta s, \Delta t)$ and $\psi_c(-\Delta s, \Delta t)$ of point S are calculated by the given hyperbolic function. In this case, the shape of the snake robot is the shape shown in Fig. 8b. Parameters $\kappa_s(0, \Delta t)$ for position $T(0, \Delta t)$ are updated as follows:

$$\kappa_s(0, \Delta t) = \kappa_c(-\Delta s, \Delta t) \tag{21}$$

Parameter $\psi_s(0, \Delta t)$ should be updated appropriately in the following manner: $\psi_s(\Delta s, \Delta t)$ at point $P(\Delta s, \Delta t)$ should have the same value as $\psi_s(\Delta s, 0)$, which belongs to the previous step. Otherwise, the snake robot generates a rolling motion by shift control. To avoid rolling motion at point P, the following equation should be satisfied :

$$\psi_s(0, 0) + \psi_s(\Delta s, 0) = \psi_s(0, \Delta t) + \psi_s(\Delta s, \Delta t) \tag{22}$$

where, $\psi_s(\Delta s, \Delta t)$ is given by

$$\psi_s(\Delta s, \Delta t) = -\psi_c(-\Delta s, \Delta t) \tag{23}$$

Therefore, $\psi_s(0, \Delta t)$ is given by

$$\psi_s(0, \Delta t) = \psi_s(0, 0) + \psi_s(\Delta s, 0) + \psi_c(-\Delta s, \Delta t) \tag{24}$$

We call this $\psi_s(0, \Delta t)$ a twisting compensation and denote it as ψ_s'.

Parameter κ_s and ψ_s' at the tail are given for every Δt by the method explained above. The shift-control method can be summarized as follows: (1) prepare queues to hold parameters $\kappa_s(s, t)$, $\psi_s(s, t)$, and $\psi_s'(s, t)$ at each segment Δs corresponding to the position on the snake robot's trunk; (2) set the initial value for each segment and input the

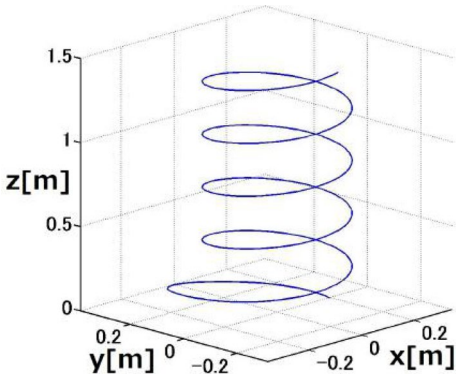

Fig. 9 An example of a helical wave curve ($A = 0.1$C$\omega = 3$C$\phi = 2\pi$, $r = 0.2$, $n = 0.05$)

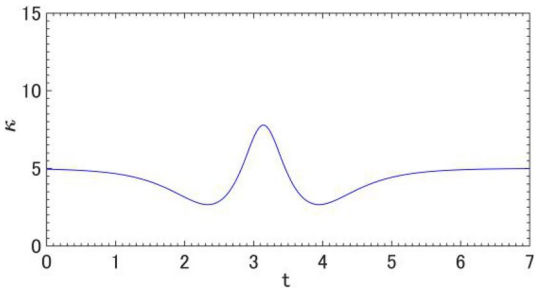

Fig. 10 The curvature κ around the protrusion of the helical wave curve ($A = 0.2$, $\omega = 2$, $\phi = 2\pi$, $r = 0.2$, $n = 0.03$)

value into the queue; (3) update the parameters of the tail position and input the new values to the first of the queue. The parameter of curvature κ_s and the twisting compensation ψ_s' are shifted to the head direction. Note that ψ_s is not shifted, but ψ_s' is shifted. Consequently, the twisting amount at s becomes $\psi_s + \psi_s'$; (4) The value in a segment corresponding to a joint position is referred to calculate the relative angle at the joint.

In this paper, the trigger to generate the floated longitudinal wave is given by a command from an operator to the snake robot.

4 Simulations

We validated the shape of the helical wave curve proposed in Sect. 3 and then conducted simulations using the Robot Operating System (ROS) and Gazebo programs. The results are shown in this section.

4.1 Shape of the helical wave curve

Examples of a helical curve that is generated from Eq. (16) are shown in Fig. 9. The curvature and torsion of the helical wave curve in Fig. 9 are shown in Figs. 10 and 11, respectively.

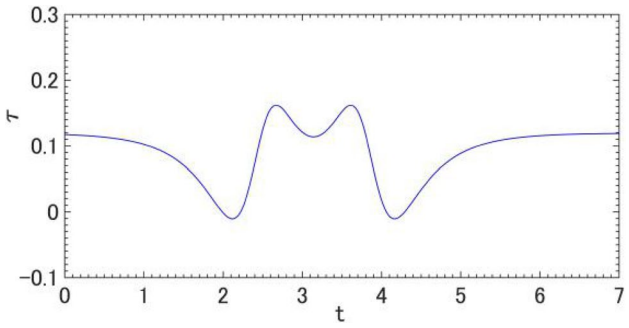

Fig. 11 The torsion τ around the protrusion of the helical wave curve ($A = 0.2$, $\omega = 2$, $\phi = 2\pi$, $r = 0.2$, $n = 0.03$)

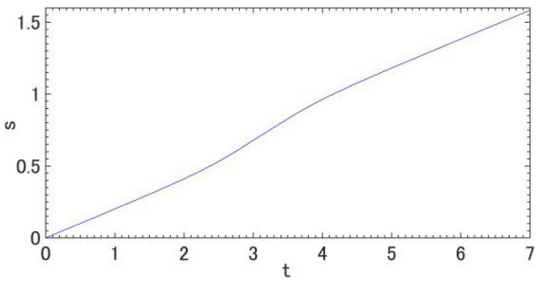

Fig. 12 The relationship between s and t around the protrusion of the helical wave curve ($A = 0.2$, $\omega = 2$, $\phi = 2\pi$, $r = 0.2$, $n = 0.03$)

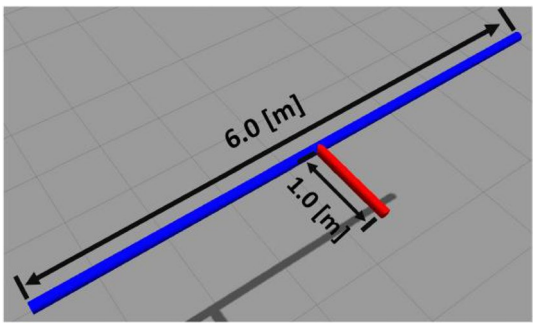

Fig. 13 Overview of the experimental pipe

An example of the relationship between s and t is shown in Fig. 12; this is calculated by substituting Eqs. (16) and (18) in Eq. (20). In Fig. 12, the slope rises where parameter t changes from 1.5 to 4.5; it corresponds directly to the floated longitudinal wave of the helical wave curve.

4.2 Simulation environment

ROS and Gazebo were used as simulation tools in this research. ROS is a package of libraries and tools to help

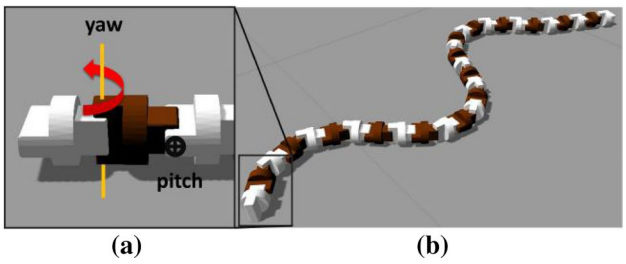

Fig. 14 Overview of the experimental snake robot and its unit

create robot applications[13, 14]. Gazebo gives us a 3D simulation tool and is designed to accurately reproduce the dynamic environments a robot may encounter[15].

The simulation environment created on Gazebo in this study is shown in Fig. 13. The radius of the pipe is 0.057 m, the length is 6.0 m, and the radius of the branch is 0.057 m; its length is 1.0 m. The pipe is placed vertically in the environment. The snake robot is constructed by connecting a mechanical unit in series. The unit has two degrees of freedom with pitch and yaw joints, as shown in Fig. 14a. The snake robot is constructed with 31 links in total, as shown in Fig. 14b. The parameters, such as the size and weight of the snake robot, are based on a real mechanical snake robot in our laboratory. The radius of the cylinder, which is a link of the snake robot, is 0.035 m, and the length is 0.061 m. The friction coefficient between the robot and pipe is set to 0.5.

4.3 Simulation results

In this simulation, the snake robot moves from the bottom to upwards using helical wave propagation. On the way to the top, there is a branch point, and the snake robot passes it successfully thanks to this type of motion. An example of the simulation results is shown in Fig. 15, where the parameters of the helical wave propagation motion are $A = 0.03$, $\omega = 1$, $\phi = 2\pi$, $r = 0.90$, and $n = 0.027$.

The angles of the head and tail joints for helical wave propagation are shown in Fig. 16. The helical wave propagation

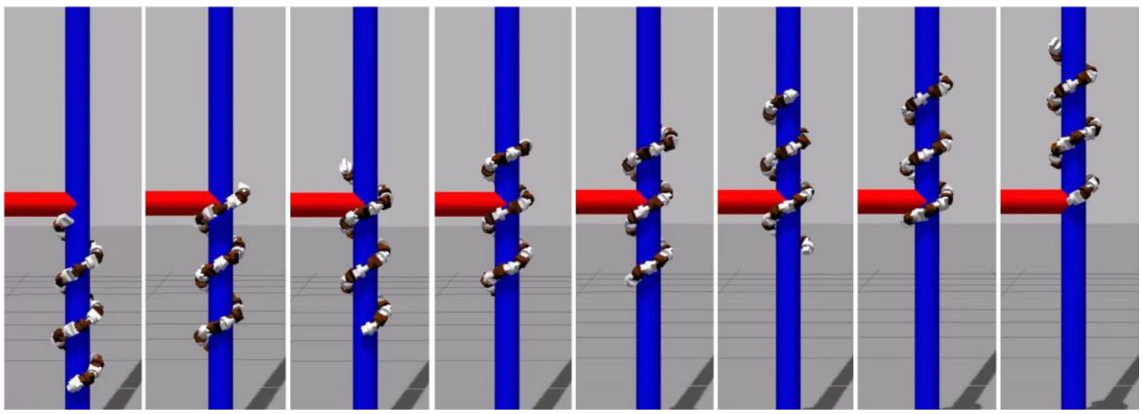

Fig. 15 An example of a simulation sequence obtained using the helical wave propagation motion. The figures are separated by intervals of approximately 22 s

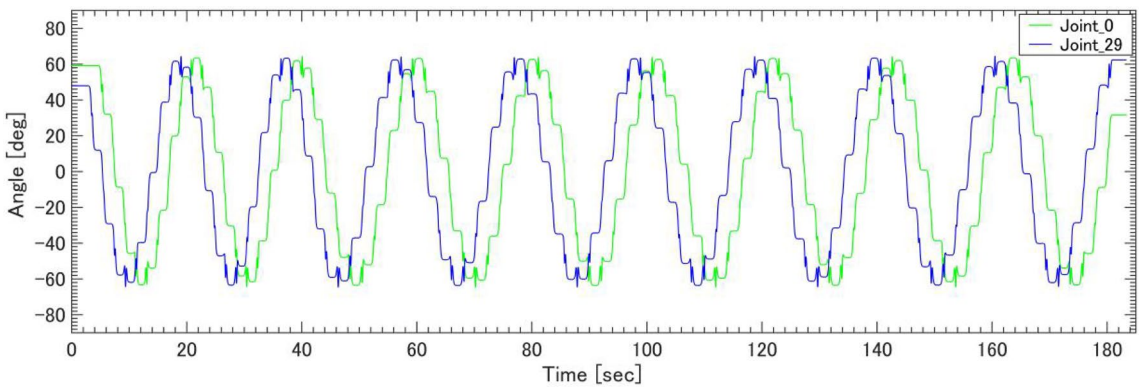

Fig. 16 The transition of angles of head and tail joints

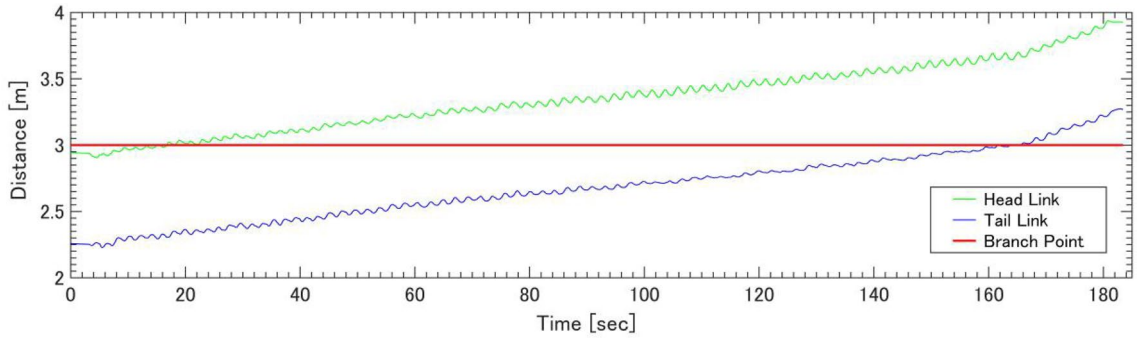

Fig. 17 The positions of the head and tail links on the z−axis in the experiment

is conducted where the angle is changing rapidly. The angles also change with a large period because of the compensation of Eq. (24). The positions of the head and tail links on the z−axis are shown in Fig. 17, in which the snake robot has successfully crossed the branch after about 170 s.

5 Conclusions

In this paper, we proposed the helical wave propagation motion as a new form of a motion for snake robots. This type of motion allows snake robots to overcome a branch point on a pipe. We adopted a hyperbolic function to make a longitudinal wave. The designed helical wave curve (in a Cartesian coordinate system) was converted into the target angles of the joints of the snake robot using the continuous curve model.

Furthermore, we conducted simulations to verify the behavior of the proposed helical wave propagation motion and confirmed that the snake robot can overcome the branch point, which is impossible to overcome using a conventional helical rolling motion.

In our simulations, the diameters of the pipe and branch, as well as the position of the branch, are known. The parameters of the controller are tuned by an operator. Future work will be devoted to examining the influence of each of the parameters of the hyperbolic function on the movement efficiency of the snake robot. We will also improve the controller to make it more adaptable and apply the helical wave propagation motion to actual machine snake robots.

Acknowledgements This research was funded by the ImPACT Program of the Council for Science, Technology, and Innovation (Cabinet Office, Government of Japan) and JSPS KAKENHI (Grant no. 15K05898).

References

1. Hirose S (1993) Biologically inspired robots (Snake-like Locomotor and Manipulator). Oxford University Press, Oxford
2. Mori M, Hirose S (2001) Development of active cord mechanism ACM-R3 with Agile 3D mobility. IEEE RSJ Int Conf Intell Robots Syst 3:1552–1557
3. Kamegawa T, Matsuno F, Chatterjee R (2002) Proposition of Twisting Mode of Locomotion and GA based Motion Planning for Transition of Locomotion Modes of 3-Dimensional Snake-like Robot. IEEE Int Conf Robot Autom 2:1507–1512
4. Date H, Takita Y (2005) Control of 3D snake-like locomotive mechanism based on continuum modeling. In: Proceedings of IDETC/CIE ASME international design engineering technical conferences and computers and information in engineering conference, pp 1351–1359
5. Rollinson D, Choset H (2013) Gait-based compliant control for snake robots. In: Proceedings of the IEEE international conference on robotics and automation, pp 5123–5128
6. Kamegawa T, Harada T, Gofuku A (2009) Realization of cylinder climbing locomotion with helical form by a snake robot with passive wheels. In: IEEE international conference on robotics and automation, pp 3067–3072
7. Baba T, Kameyama Y, Kamegawa T, Gofuku A (2010) A snake robot propelling inside of a pipe with helical rolling motion. In: Proceedings of the SICE Annual Conference, pp 2319–2325
8. Lipkin K, Brown I, Peck A, Choset H (2007) Differentiable and piecewise differentiable gaits for snake robots. In: Proceedings of the IEEE/RSJ International Conference on Intelligent Robots and Systems, pp 1864–1869
9. Mori M, Yamada H, Hirose S (2005) Design and development of active cord mechanism ACM-R3 and its 3-dimensional locomotion control. J Robot Soc Jpn 23(7):886–897 (Japanese)
10. Yamada H, Hirose S (2006) Study on the 3D shape of active cord mechanism. In: IEEE international conference on robotics and automation, pp 2890–2895
11. Hines M, Blum JJ (1983) Three-dimensional mechanics of eukaryotic flagella. Biophys J 41(1):67–79
12. Chirikjian Gregory S, Burdick Joel W (1991) Parallel formulation of the inverse kinematics of modular hyper-redundant manipulators. In: Proceedings of 1991 IEEE International Conference on Robotics and Automation, vol 1, pp 708–713
13. Quigley M et al (2009) ROS: an open-source robot operating system. CRA Workshop Open Source Softw 3(3.2):5
14. Pizarro CP, Arredondo TV, Torriti MT (2010) Introductory survey to open-source mobile robot simulation Software. In: Robotics symposium and intelligent robotic meeting (LARS), pp 150–155
15. Koenig N, Howard A (2004) Design and use paradigms for Gazebo, an open-source multi-robot simulator. In: International conference on intelligent robots and systems, pp 2150–2154